EPTT 2024
Escola de Primavera de Transição e Turbulência

ABCM
Associação Brasileira de Engenharia e Ciências Mecânicas

EPTT-2024-0026
BOUNDARY LAYER TRANSITION AFFECTED BY A GAP

Victor B. Victorino
Felipe O. Aguirre
Lenz J. L. Lazaro
São Carlos School of Engineering, University of São Paulo - Av. Trabalhador São Carlense, 440. Zip code: 13566-590
barcelos.victorino@usp.br
felipe.aguirre@usp.br
lenzjll@usp.br

Marcello A. F. Medeiros
São Carlos School of Engineering, University of São Paulo - Av. Trabalhador São Carlense, 440. Zip code: 13566-590
marcello@sc.usp.br

Abstract. *The present paper experimentally investigates how a gap affects the boundary layer stability and transition. The experiments were carried out in a low turbulence intensity wind tunnel and the experimental rig consisted of a cavity with interchangeable depth inserted on a flat plate. We employed hot wire anemometry for measuring velocity and a Preston tube to determine the transition location. Results showed that a shallow gap does not significantly affect the transition. Strong destabilization of the T-S waves was observed from a gap deeper than a certain threshold, including traces of non-linear growth. As the gap depth continued to increase, the destabilization of T-S waves and the shift in transition location tended to remain saturated by this non-linear regime. Ultimately, the Rossiter mode emergence was identified, and when it reached large amplitudes, promoted an abrupt transition at the gap trailing edge.*
Keywords: *Gap, Cavity, Tollmien-Schlichting waves, Transition, Rossiter mode.*

1. INTRODUCTION

Turbulence in many applications can be a desirable feature, however, it also presents disadvantages. In the Aeronautics field, the skin friction drag is significantly increased by a turbulent boundary layer on aerodynamic surfaces, such as a wing, and as a consequence, the aerodynamic efficiency is penalized. Therefore, to produce more efficient wings, turbine blades, propellers, etc., engineering has an interest in avoiding turbulent boundary layers over these surfaces.

In a lowly disturbed flow, the laminar boundary layer undergoes laminar-turbulent transition via the growth of Tollmien-Schlichting (T-S) waves (Schubauer and Skramstad, 1948; Saric *et al.*, 2002), the primary viscous instability mode of a two-dimensional boundary layer. Although low-amplitude T-S waves spatially grow linearly during the early stages of the unstable region, non-linear mechanisms play an important role in the turbulent breakdown as they get larger amplitudes (Crouch, 2006). The Literature reports different types of turbulent breakdown: the fundamental (Klebanoff *et al.*, 1962), the sub-harmonic (Herbert, 1988; Kachanov and Levchenko, 1984), and the oblique (Craik, 1971; Berlin *et al.*, 1994). The non-linear nature of the transition difficult to predict the transition location, required to accurately predict the drag of an aircraft or suit a numerical mesh for simulations, for instance. As a consequence, much effort is spent to study the boundary layer stability and transition.

Since the non-linear regime is sharp relative to the linear region, the linear hypothesis offers a fairly suitable way to model the growth of the T-S waves. That idea is the base for amplitude-based methods to predict the transition, such as the e^N methods (van Ingen, 1956; Smith and Gamberoni, 1956) According to this method, transition takes place where the T-S linear amplification factor, $\int_{x_0}^{x} -\alpha_i(x)dx$, reaches a value, N, through correlation with experiments. However, the presence of surface irregularities, widely present in many practical applications, often requires additional correlations to correct the transition criteria (Forte *et al.*, 2015; Beguet *et al.*, 2017; Crouch and Kosorygin, 2020), usually based on some parameter related to the surface irregularity geometry. Amid the canonical surface irregularities reported in the Literature (Tani *et al.*, 1954; Klebanoff and Tidstrom, 1972; Wang and Gaster, 2005), the present paper deals specifically with gaps, which are open cavities with their dimensions with the order of magnitude close to the boundary layer thickness over the cavity leading edge. This paper will use the nomenclature gaps to differentiate from the open cavity, which focuses more on the flow near the interior region of the cavity. Oppositely, the present paper addresses the boundary layer downstream

of the gap, rather than the mixing layer inside the cavity. As well as the other surface irregularities, a gap destabilizes the T-S waves, shifting the transition upstream, until it eventually reaches the cavity. In this manner, one of the simplest approaches consists of determining a deficit in the amplification factor ΔN due to the destabilization promoted by the gap. By definition, $\Delta N = N_{(D=0)} - N_{gap}$. Nonetheless, under some circumstances, the growth of T-S waves can be bypassed by another mechanism that triggers transition right at the trailing edge of the gap (Forte *et al.*, 2015; Beguet *et al.*, 2017; Crouch *et al.*, 2022). On the regime where the gap affects the T-S wave, Forte *et al.* (2015) reported that the gap width L (streamwise) produces more impact on the T-S rather than the depth D, therefore, it was the reference length chosen. Crouch *et al.* (2022) also found that the largest ΔN occurs for relatively greater values of L/δ^*. Forte *et al.* (2015) and Beguet *et al.* (2017) break the ΔN down into two parcels: a peak that is associated with the gap near-field (ΔN_{peak}) and a positive shift quasi-parallel to the original curve (ΔN_{far}). The authors revealed that the N_{peak} is associated with high frequencies, that decay abruptly in a short space downstream of the gap. On the other hand, the N_{far} seemingly is the scar of the gap on the T-S growth. There is a conceptual difference between the models from ONERA (Forte *et al.*, 2015; Beguet *et al.*, 2017) and Crouch *et al.* (2022). Forte *et al.* (2015) and Beguet *et al.* (2017) model the ΔN taking into account the Reynolds number based on the gap width Re_L and the momentum thickness at the gap Re_{θ_g}, whereas, Crouch *et al.* (2022) overlook the effect of the Reynolds number. Crouch *et al.* (2022) takes into account only the geometry of the gap normalized by the displacement thickness of the boundary layer at the gap leading edge.

As previously mentioned, Forte *et al.* (2015), Beguet *et al.* (2017), and Crouch *et al.* (2022) reported the presence of the so-called tripping or bypass limits. Such a threshold is indicated by a L-shaped curve in a diagram with respect to D/δ^* and L/δ^*. Beguet *et al.* (2017) is more conservative and indicated the tripping limits as the region comprehended by $L/\delta^* \geq 18$ and $D/\delta^* \geq 2$. The threshold from Crouch *et al.* (2022) presents some nuances, with a slightly inclined boundary within the range of $19 \leq L/\delta^* \leq 36$. Analyzing the cavity oscillation threshold from Sarohia (1977), we can see similarities with these reported bypass transition limits. However, Sarohia (1977) does not provide details regarding where the measurements took place. Also, Crouch *et al.* (2022) measured a high-frequency tonal in one case where bypass transition occurred. That raised the question, of whether such a tonal could be linked to the Rossiter instability (Rossiter, 1964). The supposition that the Rossiter mode possibly triggers transition was numerically investigated by Victorino *et al.* (2023). The LST results indicated that the neutral limits of the Rossiter modes were close to the bypass limits from Crouch *et al.* (2022) and the frequency of the Rossiter agreed within 1% with the oscillation experimentally measured by them. The bypass bounds are greater than the Rossiter neutrality. The LST results also showed that the Centrifugal modes (Brés and Colonius, 2008) neutral limits are lower than the Rossiter's in this parametric space. The DNS data from Victorino *et al.* (2023) revealed that neither a strong centrifugal nor a strong Rossiter mode alone produces turbulence. However, the gap triggers the transition when both modes are unstable. Furthermore, the Rossiter instability, when increased, shifted the transition toward the gap.

The objective of this study is to experimentally investigate how a gap can influence the boundary layer transition. We present the results of a gap with varying depth (D), constant length (L), and constant Reynolds at the gap leading edge (Re_{δ^*}). The choice for the parametric space covered in this paper was based on the Literature, numerical results performed by our research group, and preliminary experiments. We seek to experimentally evidence traces of the Rossiter mode as a transition-promoting mechanism as well as characterize the natural (unforced) destabilization caused by a gap in the growth of the Tollmien-Schlichting waves.

2. Experimental setup

The experiments were performed in the Low Acoustic Noise and Turbulence (LANT) wind tunnel (Amaral *et al.*, 2021) located at the São Carlos School of Engineering, University of São Paulo. The LANT is a closed-circuit wind tunnel with a closed and squared test section of 1 m $\times$ 1 m $\times$ 3 m, capable of reaching a maximum free-stream velocity up to 42 m/s (empty test section) with a turbulence intensity of 0.036% (1-1024 Hz) and flow uniformity within less than $\pm 0.4\%$ around the centerline. The test model is schematically represented in Fig. 1. It is composed of an aluminum flat plate with dimensions 2000 mm (chord) $\times$ 999 (span) mm $\times$ 10 mm (thickness) attached to an asymmetric leading edge (Hanson *et al.*, 2012) and also to a flap/trim tab set in its trailing edge to fine-tuning the pressure distribution over the flat plate. The entire assembly of the model presents a total chord of 2.32 m. The model is vertically installed inside the test section. The gap rig is composed of a retractable part driven by a lead screw linear assembly driven by two stepper motors connected in parallel. Such a mechanism is attached to an insert plate mounted flush with the main flat plate. The insert presents a cut-out where the cavity bottom travels producing a depth capable of reaching ± 20 mm (the rig can also form a sharp-edged protrusion). The cut-out has a sharp-corners rectangular shape with dimensions 600 mm $\times$ 30 mm, corresponding to the gap width (b) and the gap length in the flow direction (L). The gap leading edge x_g is located at 600 mm distant from the model's leading edge. A three-dimensional Cartesian traverse comprises one of the lateral walls of the test section and is responsible for positioning the flow measurement sensors. The spatial resolution of the wall-normal axis y is 6.25 μm. A 3D-printed wing covers the traverse bar to avoid undesired oscillations induced by the cylindrical rod exposed to the flow.

The velocity measurements were performed through the hot wire anemometry technique (constant temperature mode).

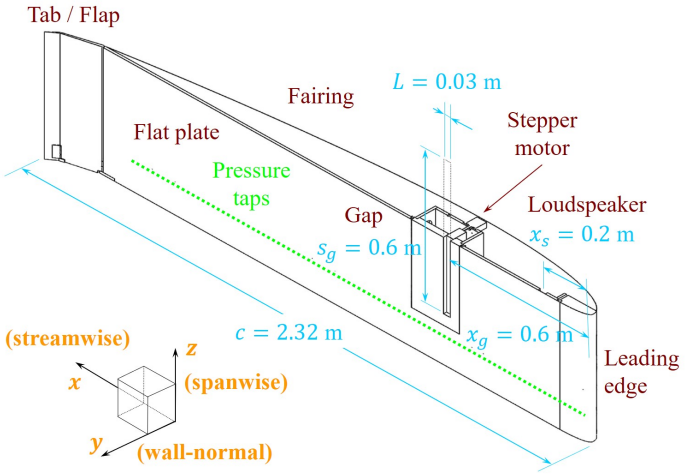

Figure 1: Section view of the model employed in the experiments

The anemometer circuit employed was the AN-1002 from A.A. Lab System, while the probe was the miniature wire boundary layer probe 55P15 with a 5 μm diameter from Dantec Dynamics. The output voltage from the hot wire feeds three instruments: (i) a digital oscilloscope with a voltmeter embedded, (ii) a PXI 4496/98 board from National Instruments (NI) embedded in a 1042Q chassis, and (iii) a NI DAq-USB 6002. The first allows real-time visualization of the raw signal. The latter instruments are responsible for signal recording. We use the PXI 4496/98 board to acquire the fluctuation signal since it presents a higher resolution (24-bit) and lower noise than the NI DAq-USB 6002. Since this instrument has a high-pass filter to remove the mean component, the signal to DAq-USB 6002 is employed to record the mean output voltage from the HWA. Additionally, the multi-role capacity of the DAq-USB 6002 allows one to use its digital ports to control other systems such as the stepper motors drivers from the traverse and the interchangeable gap mechanism.

A Preston tube was employed to detect the transition. Such an instrument consists of a 0.9 mm diameter tube that captures the total pressure over the flat plate surface. The tube is bent with a shape similar to the boundary layer hot wire probe, to reach the wall with a small contact angle. On the tip of the traverse wing, an LVDT linear displacement sensor maintains the contact angle constant during a streamwise scan. The static ports from a Pitot tube installed on the traverse wing are used to measure the free-stream static pressure, to calculate the dynamic pressure from the Preston tube. The total and static pressures feed, through tubes, a differential pressure transducer RSC series from Honeywell, with uncertainty of ± 1.25 Pa. Figure 2 exhibits a Preston tube streamwise scan over the flat plate containing a gap. The dynamic pressure of the flow close to the wall is proportional to the skin friction coefficient, $c_f = \tau_w / q_\infty$. Since the wall shear stress is inversely proportional to the boundary layer thickness, the skin friction coefficient decreases as it develops in the streamwise direction. However, when the boundary layer undergoes transition, the velocity profile suddenly changes, with its derivative with respect to the wall-normal direction becoming steeper at the wall. As a result, the dynamic pressure (skin friction coefficient) abruptly increases. Thus, it is possible to determine the location of the transition. The dashed and dotted lines show fitted curves that illustrate the laminar and transitional behavior of the skin friction coefficient, respectively. Ultimately, the transition is graphically determined as the most downstream location before a steep rise in the skin friction coefficient. According to Fig. 2, the transition location was determined at (x = 1.76 m) and is highlighted by the red marker.

3. Preliminary experiments

The pressure distribution, shown in Fig. 3 exhibits that the stagnation is located on the working side of the model. A weak suction peak occurs in $x = 90$ mm, and then a slight adverse pressure develops up to $x = 300$ mm. This does not affect the stability, since the Re_{δ^*} at that location is below the critical Re_{cr} for the flow conditions employed. The pressure distribution in the remaining extension of the flat plate is nearly constant, with a mildly favorable bias that can be related to the Falkner-Skan parameter m (Schlichting, 1979). It was estimated that the pressure distribution reasonably agrees with $m = 0.01$. This parameter does not significantly affect the mean profile, however, it can affect the integral linear growth rate, as will be discussed next. Therefore, to compensate for the small global pressure gradient effect, and consequently, compute the equivalent Blasius profile, we follow the technique proposed by Saric (1990), where the compensated x position is obtained by computing a virtual leading edge distance x_v value that matches the Blasius and the experimentally measured displacement thickness as $x_v = (1.72/\delta^*_{meas})^2 (U_\infty/\nu)$.

Figure 4 exhibits a comparison of the mean boundary layer profile (Fig. 4a) and the disturbance velocity profile

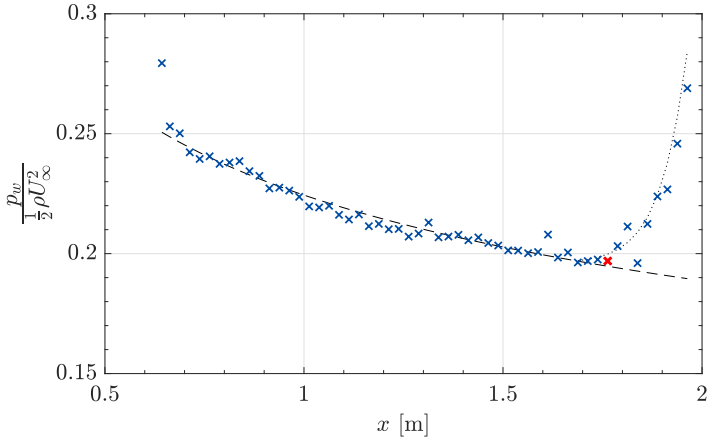

Figure 2: Distribution of dynamic pressure close to the flat plate wall measured with a Preston tube ($U_\infty/\nu = 1.66 \times 10^6$). Red marker corresponds to the estimated transition location.

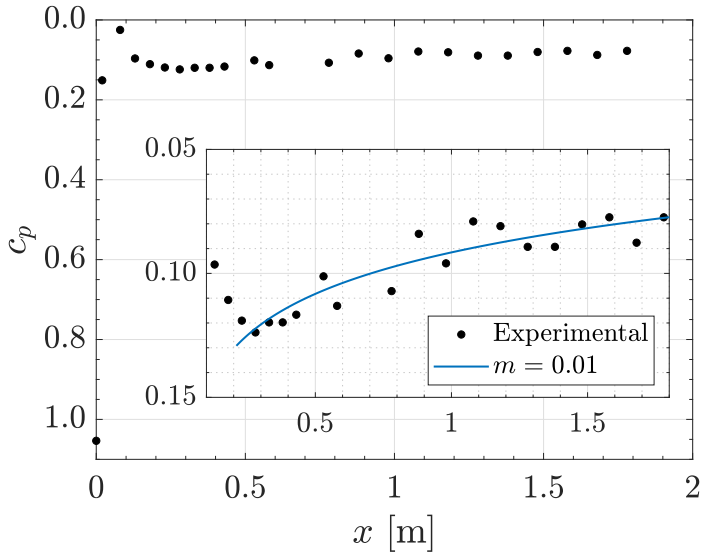

Figure 3: Pressure coefficient distribution over the model's working side.

(Fig. 4b), with the theoretical Blasius profile and the Tollmien-Schlichting eigenfunction, respectively. Concerning the profile comparisons, good agreement was observed in both measurements. The maximum x_v computed deviated from the geometric by 10% at the most downstream position. The contours shown in Fig. 4a represent the normalized velocity U/U_∞ distribution along the wall-normal coordinate ($\eta = y\sqrt{U_\infty/\nu x}$) and spanwise direction z. To determine the experimental velocity disturbance, the methodology followed was similar to Methel *et al.* (2022). The disturbance velocity signal in each coordinate was analyzed in the spectral domain, which presented a bulge of amplified frequencies that matched the T-S unstable band for the local Reynolds $Re_{\delta^*} = 2440$. The band of amplified frequencies presented a bell-shaped distribution and the center of that peak was around $f = 132$ Hz ($2\pi f \delta^*/U_\infty = 0.088$). Since the signal processing can introduce scattering, the amplitudes for each y location were obtained as the average amplitude in the frequency range of $112 \leq f \leq 152$ Hz. The natural T-S amplitude distribution was not perfectly two-dimensional, thus the profile exhibited by the green markers is the result of the average of the profiles along the range of ± 90 mm around the centerline. The profile was normalized so the outer peak matched the theoretical result in each z location. In that manner, we were able to compare the T-S experimental disturbance profile with a theoretical eigenfunction obtained from an in-house Orr-Sommerfeld solver, based on Juniper *et al.* (2014), for a Blasius boundary layer with the same values of Re_{δ^*} and $\omega = 0.088$.

Figure 5 compares the envelope of the theoretical amplification factor and that measured experimentally. The natural logarithm of the normalized amplitudes with respect to the amplitude at $x = 0.65$ m has been taken. Note that as the initial position of the $x = 0.65$ measurements is already above the critical Re_{δ^*}, the experimental curve was shifted to make the data match the theoretical curve. The theoretical calculation was made by solving the Orr-Sommerfeld equation using the Reynolds number values corresponding to the experiment. The velocity profile used was the Falkner-Skan profile with

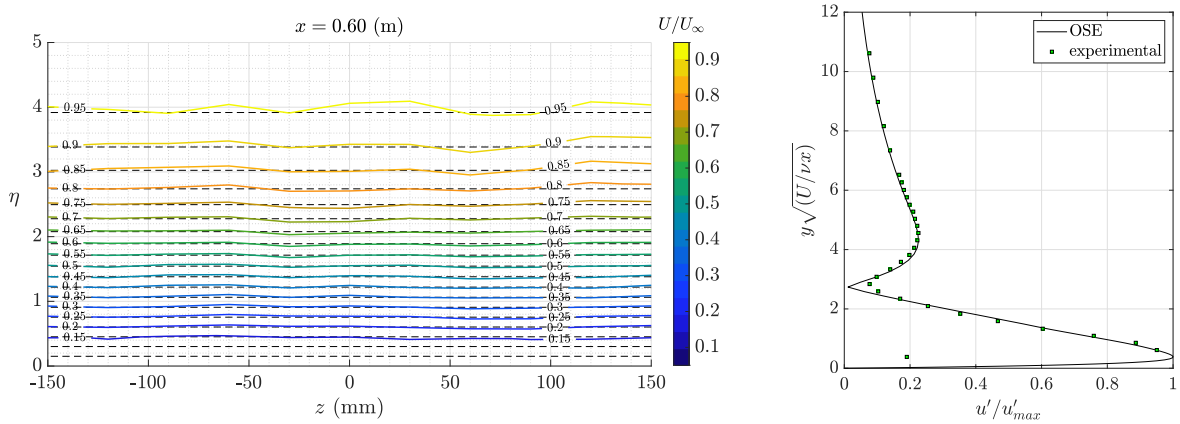

(a) (b)

Figure 4: (a) Contours of the normalized mean velocity profile along the span at $x = 0.60$ m. Black dashed lines exhibit the Blasius profile. (b) Experimental amplitude profile of the fluctuation velocity (symbols) compared to the theoretical Tollmien-Schlichting eigenfunction (solid) from OSE solution for local condition at $x = 1.75$ m.

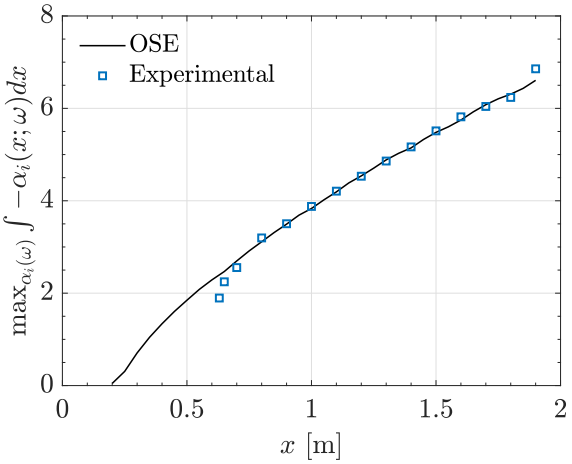

Figure 5: Comparison between the theoretical and experimental amplification factor envelope.

the parameter $m = 0.01$. The amplification rates were scaled with the local value of the boundary layer thickness given the flow conditions of the experiment and integrated according to Eq. (1).

$$n(x) = \ln\left(\frac{A}{A_0}\right) = \max\left[-\int_{x_0}^{x} \alpha_i(x;\omega)dx\right] \tag{1}$$

In the integration, for each value of x, the maximum amplification rate α_i was used as a function of the dimensionless circular frequency $\omega = 2\pi f \delta^*/U_\infty$. The frequency range used was $100 - 560$ Hz in both the theoretical and experimental cases.

4. The influence of a gap on the Tollmien-Schlichting wave growth

A streamwise sweep of the disturbance velocity for various gap depths was carried out. The hot-wire probe was located at a wall distance where the mean velocity profile matches $U/U_\infty = 0.4$ in the smooth flat plate. The signal was collected during 30 s in each measurement station. Signals were processed in the frequency domain to be compared to the theory. Welch's method (Bendat and Piersol, 2010) was used to smooth the spectra. It consists of dividing the time series into smaller blocks, applying a Hanning window on each segment, and ultimately, taking the average power spectral density (PSD) from all the blocks. Next, the energy correction factor for the windowing used ($\sqrt{8/3}$) was applied, and finally, the square root of the PSD was taken, yielding a smoothed Fourier amplitude spectrum. The spectra presented were compared with the theory. To perform such analysis, the spatial axis x was re-scaled as Reynolds number $Re_{\delta^*} = U_\infty \delta^*/\nu$ using the value of the boundary layer thickness for each position x. Since the displacement thickness was only measured in $x = x_g = 0.6$ m, the displacement thickness in the remaining position was obtained according

to $\delta^* = \delta^*_{ref}\sqrt{(U_{ref}\nu x)/(U\nu_{ref}x_{ref})}$. On the other hand, frequencies have been scaled as $F = 2\pi f\nu/U^2_\infty(10^6)$. In this manner, the non-dimensional frequency has no dependence on the boundary layer thickness, and as a consequence, horizontal lines correspond to a constant dimensional frequency. Figure 7 exhibits the contours of the Fourier magnitudes in logarithmic scale. The gap trailing edge corresponds to the left end of the contours. The plot also shows two theoretical stability limits using two different forms of modal analysis: (i) the Parabolic Stability Equation (PSE) and (ii) the Orr-Sommerfeld Equation (OSE), developed by the group based on Juniper *et al.* (2014). The former takes into account the non-parallel effect whereas the latter does not. However, minor differences in the stability limits occurred, particularly for frequencies in the range $F \leq 100$.

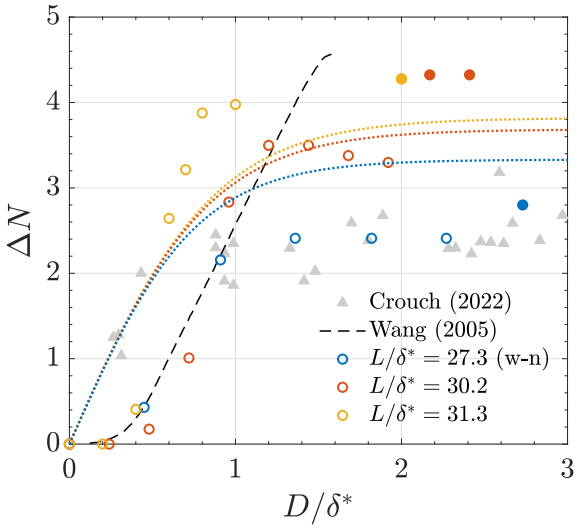

Figure 6: Amplification factor variation ΔN as a function of the normalized depth D/δ^*.

Contours shown in Fig. 7a correspond to the spectra of the smooth flat plate. It was possible to confirm that the lobe of amplified disturbances attributed to T-S waves, indeed rely on the theoretically unstable region, showing a good agreement. The dominant frequency $F = 31$ is responsible for causing the transition in the smooth flat plate. Figures 7b and 7c exhibit a progressively, yet mild, destabilization of the T-S wave due to the gap. The gap with $D/\delta^* = 0.75$, shown in Fig. 7d, exhibits that the transition was strongly affected and the dominant frequency changed to a relatively low-frequency, with a value close to the sub-harmonic of the dominant one. Results suggest that the gap with $D/\delta^*_g = 0.75$ anticipated the non-linear growth of the sub-harmonic. Figures 7e, 7f, 8a, and 8b show the regime where the gap massively destabilizes the T-S, producing turbulence at the gap's trailing edge, which does not sustain and spatially decays. Seemingly, the separated flow confined within the gap is turbulent. However, the mean profiles past the reattachment in the gap trailing edge present a shape that confers stability. Such assertion is based on Preston tube readings, which show a smooth increase in skin friction, and also based on numerical data for similar parameters. Although, the mean velocity profile was not experimentally measured downstream of the gap. Hence, the turbulence produced in the mixing layer can not be sustained and abruptly decays. Yet, this turbulence affects the T-S amplitude, triggering non-linear growth of the fundamental and sub-harmonic modes. As a result, the transition is anticipated.

Following the methodology from Crouch *et al.* (2022), the transition location determined by the Preston tube data projected into the amplification factor envelope for the smooth flat plate is capable of estimating the ΔN caused by the gap. Figure 6 shows the values of the deficit in the N factor (markers) caused by the gap, $\Delta N = N_{D=0} - N_g$. The results partially agree with those of Crouch *et al.* (2022). The impact of gap depth on the transition to values in the $D/\delta^*_g \leq 1$ range was less than the measured by Crouch *et al.* (2022). The results of this experiment show that for very small values of depth ($D/\delta^*_g \leq 0.5$), cavities in the range $28 \leq L/\delta^* \leq 30$ have a negligible impact on ΔN. This is not the case in Crouch *et al.* (2022). However, the deep-gap limit was also observed and the value was slightly higher than the results measured by Crouch *et al.* (2022). According to the Crouch *et al.* (2022) model, the deficit in the N factor can be represented by the following equation.

$$\Delta N = 0.122\left(\frac{L}{\delta^*_g}\right)\tanh\left(36\frac{D}{L}\right) \tag{2}$$

This model is represented graphically in Fig. 6 for $L/\delta^* = 28$ and 31 (extremes) by dashed lines. According to the authors, their model is conservative. It can be seen that the curves lie above their experimental values. However, the results of the present experiment are close to the correlation stipulated by the model, for depth values $D/\delta^* > 1$. Additionally, the adverse pressure gradient imposed by Crouch *et al.* (2022) is destabilizing, whereas, the present is slightly favorable.

In that way, in the adverse pressure gradient, the T-S waves grow in a relatively short space compared to a favorable pressure gradient. This difference may explain why the ΔN for a deep-gap limit was greater in the present. Additionally, since a less destabilizing pressure gradient was observed in the present, the threshold for non-linear growth may occur with a deeper gap, shifting the ΔN curve to the right. Notably, the present ΔN function calculated lies close to the backward-facing step correlation from Wang and Gaster (2005) for gaps with small depths. However, for deeper gaps the ΔN tends to saturate and deviate from the correlation by Wang and Gaster (2005), similarly to the so-called deep-gap limit reported by Crouch *et al.* (2022). Also, the saturation level increases with L/δ^*, as reported by Crouch *et al.* (2022).

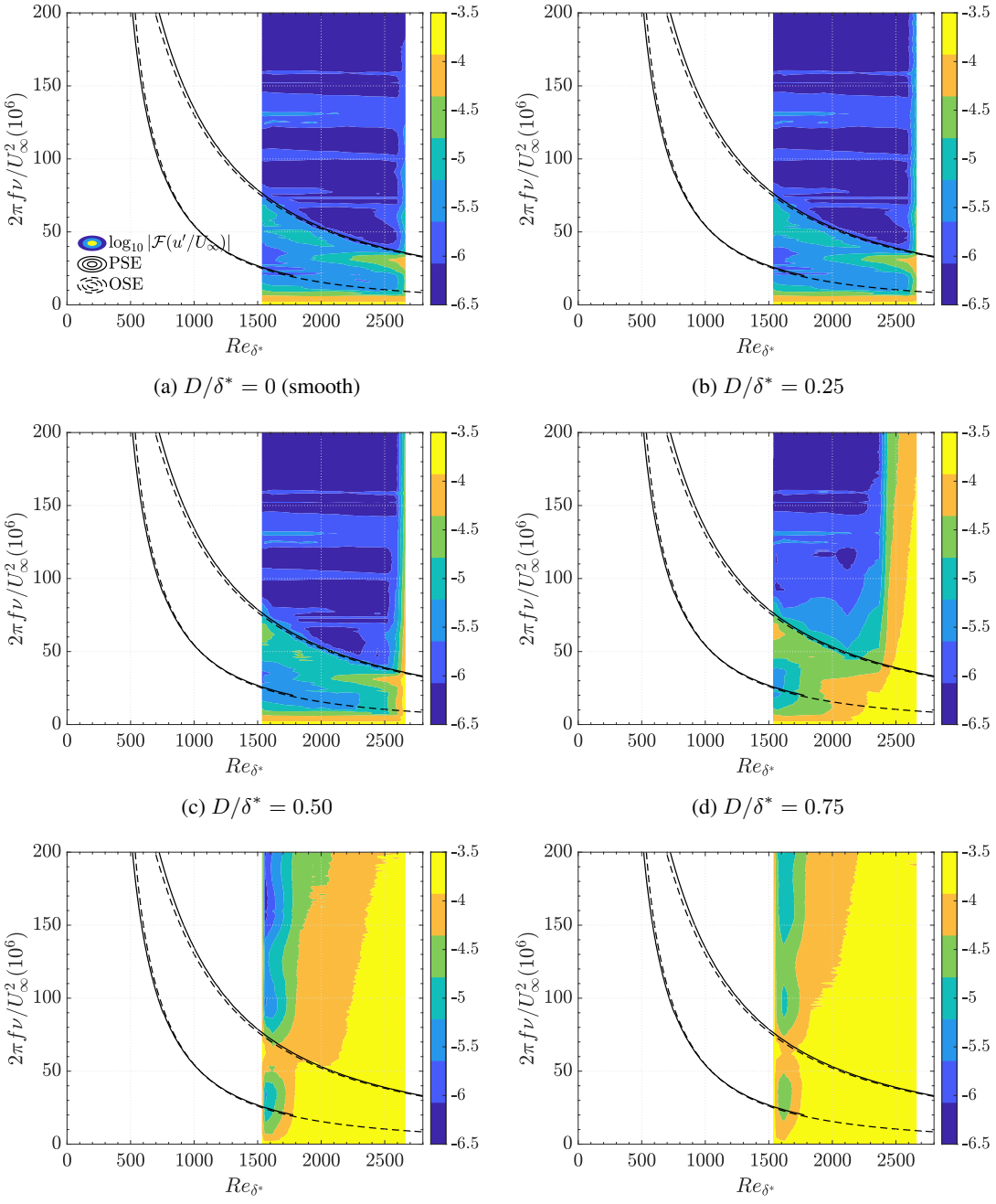

(a) $D/\delta^* = 0$ (smooth)

(b) $D/\delta^* = 0.25$

(c) $D/\delta^* = 0.50$

(d) $D/\delta^* = 0.75$

(e) $D/\delta^* = 0.99$

(f) $D/\delta^* = 1.24$

Figure 7: Magnitudes of the Fourier spectrum compared to Linear Stability Theory.

5. Rossiter mode triggering laminar-turbulent transition

Figure 8 exhibits the progression of the gap in the stages close to the bypass transition. The contours shown in Fig. 8a and Fig. 8b display an amplification quite similar to the exhibits in Fig. 7f, evidencing the so-called deep-gap limit, where the ΔN saturates as the gap gets deeper. The results suggest that the gap confines the separation, differently from

other surface irregularities, such as a backward-facing step or a bump. Thus, a turbulent separation at the gap leading edge passes through a phenomenon similar to a relaminarization past the accelerated flow at the gap trailing edge. Although that process leaves a scar in the T-S, the progression is similar. Possibly, both the destabilization and relaminarization intensities are evenly proportional to the gap depth, resulting in a similar net effect in the transition. That can explain the fact that the gap evidences the deep-gap limit reported by Crouch *et al.* (2022).

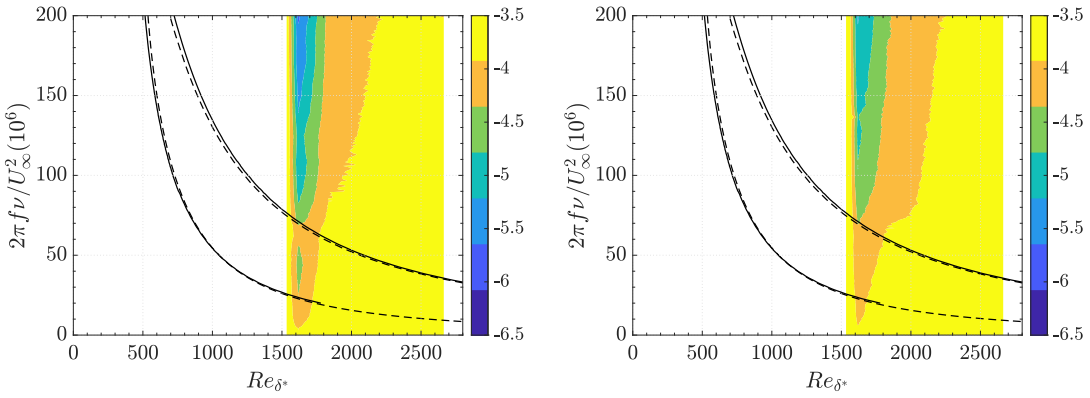

(a) $D/\delta^* = 1.74$ (b) $D/\delta^* = 1.99$

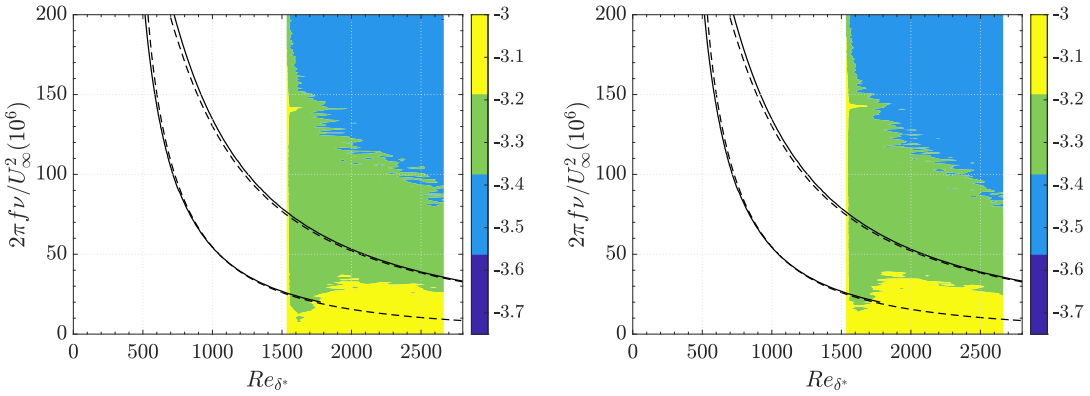

(c) $D/\delta^* = 2.24$ (d) $D/\delta^* = 2.49$

Figure 8: Magnitudes of the Fourier spectrum compared to Linear Stability Theory close to bypass transition. Note that the contours in (c) and (d) are different from the others.

Figure 8b marks the onset of a weak Rossiter mode with a frequency of $F = 134$. Furthermore, the coexistence of T-S and Rossiter modes was observed. It has to be stressed that the Rossiter frequency occurs close to the T-S first fundamental frequency of the dominant band, in the range $40 \leq F \leq 80$, locally at $Re_{\delta^*} \approx 1300$. A resonance between the Rossiter mode and the non-linear T-S can occur in the parametric space investigated. However, the Rossiter vortices do not sustain themselves as they are convected downstream, decaying abruptly. Ultimately, Fig. 8c and Fig. 8d exhibit the streamwise disturbance when bypass transition occurs. Note that the contour levels are different. In the present, the Rossiter non-dimensional frequency varied within the range $130 - 140$, depending on the gap depth, occurring near the frequency of $F = 163$ pointed by Crouch *et al.* (2022) in a case where bypass transition occurred. The Rossiter frequency is inversely proportional to the cavity length, thus, the lower frequency in the present agrees with the behavior predicted by Rossiter (1964), since the gap was longer ($L/\delta^* = 30$) than the observed by Crouch *et al.* (2022) ($L/\delta^* = 20$). Data also suggests that a strong Rossiter mode was the mechanism that led the boundary layer to transition, agreeing with numerical and theoretical results from Victorino *et al.* (2023). Their results indicated that the Rossiter mode must reach a certain level of instability to cause the transition and this was also verified in the experiments since the incidence of a weak Rossiter in the gap with $D/\delta^* = 1.99$ was not sufficient to bypass the transition. The Rossiter mode presented a frequency that matched the predicted by the LST in similar parametric space, lying in the range $\omega = 0.20 - 0.24$.

6. Final remarks

The present study experimentally investigates the destabilization effect that a gap causes in the boundary layer and its transition. Preliminary experiments were carried out to characterize the base and disturbance flow. Figure 9 summarizes the effect of the gap at the near field. Contour plots of the PSD are projected into the bottom plane of the plot box to

aid the visualization. For shallower gaps, a slight destabilization of the T-S waves is observed. As the depth increases, a strongly non-linear regime was observed before the full development of the Rossiter mode bypassing the growth of T-S waves as a transition-promoting mechanism. It was observed that the Rossiter mode needs to reach a certain amplitude before causing transition. For deeper gaps ($D/\delta^* \geq 10$ in Fig. 9), a stabilization of the Rossiter mode was observed, yet, a rapid transition is still occurring. The ΔN was compared to the Literature, exhibiting concordance in some aspects, but diverging in others. The different pressure gradients over the flat plate may explain the differences. The so-called deep-gap limit by Crouch *et al.* (2022) seems to be related to the confinement of the separation bubble due to the geometry of a gap. A phenomenon similar to a relaminarization showed that the turbulence in the separated flow over the gap does not sustain far downstream from the reattachment in the flat plate, rapidly decaying. The present results provided experimental evidence to numerical studies by Victorino *et al.* (2023) that showed that the Rossiter mode causes the laminar-turbulent transition after it reaches a determined amplitude.

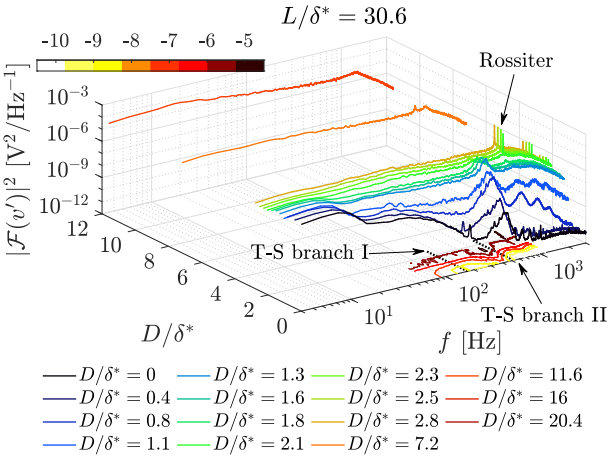

Figure 9: Spectra evolution of the fluctuation velocity as a function of the gap depth for $L/\delta^* = 30.6$.

7. ACKNOWLEDGEMENTS

V.B.V., F.O.A., and L.J.L.L thank the Coordination of Superior Level Staff Improvement (CAPES) for the scholarship. M.A.F.M. thanks the National Council for Scientific and Technological Development (CNPq) grant no. 307956/2019-9, the Agency for Financing Studies and Projects (FINEP) grant no. 01.09.0334.04, The Sao Paulo Research Foundation (FAPESP) grant no. 2019/15366-7, The Boeing Company grant no. 2021-GT-353, and the US Air Force Office of Scientific Research (AFOSR) for grants FA9550-18-1-0112, managed by Dr. Geoffrey Andersen under supervision by Lt. Col. Daniel Montes from SOARD, and FA9550-23-1-0030, managed by Dr. Roger Greenwood.

8. REFERENCES

Amaral, F.R., Serrano Rico, J.C., Bresci, C.S., Beraldo, M.M., Victorino, V.B., Gennaro, E.M. and Medeiros, M.A., 2021. "The low acoustic noise and turbulence wind tunnel of the University of Sao Paulo". *Aeronautical Journal*, Vol. 126, No. 1297, pp. 500–532. ISSN 00019240. doi:10.1017/aer.2021.80.

Beguet, S., Perraud, J., Forte, M. and Brazier, J.P., 2017. "Modeling of transverse gaps effects on boundary-layer transition". *Journal of Aircraft*, Vol. 54, No. 2, pp. 794–801. ISSN 00218669. doi:10.2514/1.C033647.

Bendat, J.S. and Piersol, A.G., 2010. *Random data: analysis and measurement procedures*. John Wiley & Sons, 4th edition. ISBN 0470248777.

Berlin, S., Lundbladh, A. and Henningson, D., 1994. "Spatial simulations of oblique transition in a boundary layer". *Physics of Fluids*, Vol. 6, No. 6, pp. 1949–1951. ISSN 1070-6631. doi:10.1063/1.868200. URL `https://doi.org/10.1063/1.868200`.

Brés, G.A. and Colonius, T., 2008. "Three-dimensional instabilities in compressible flow over open cavities". *Journal of Fluid Mechanics*, Vol. 599, pp. 309–339. ISSN 00221120. doi:10.1017/S0022112007009925.

Craik, A.D., 1971. "Non-linear resonant instability in boundary layers". *Journal of Fluid Mechanics*, Vol. 50, No. 2, pp. 393–413. ISSN 14697645. doi:10.1017/S0022112071002635.

Crouch, J., Kosorygin, V., Sutanto, M. and Miller, G., 2022. "Characterizing surface-gap effects on boundary-layer transition dominated by tollmien–schlichting instability." *Flow*, Vol. 2 (E8). doi:10.1017/flo.2022.1.

Crouch, J.D., 2006. "Instabilities in boundary-layer flows and their role in engineering". In G.E.A. Meier, K.R. Sreeni-

vasan and H.J. Heinemann, eds., *IUTAM Symposium on One Hundred Years of Boundary Layer Research*. Springer Netherlands, Dordrecht, pp. 105–114. ISBN 978-1-4020-4150-1.

Crouch, J.D. and Kosorygin, V.S., 2020. "Surface step effects on boundary-layer transition dominated by tollmien–schlichting instability". *AIAA Journal*, Vol. 58, No. 7, pp. 2943–2950. doi:10.2514/1.j058518.

Forte, M., Perraud, J., Seraudie, A., Beguet, S. and Casalis, L.G.G., 2015. "Experimental and Numerical Study of the Effect of Gaps on Laminar Turbulent Transition of Incompressible Boundary Layers". *Procedia IUTAM*, Vol. 14, No. 0, pp. 448–458. ISSN 22109838. doi:10.1016/j.piutam.2015.03.073. URL `http://dx.doi.org/10.1016/j.piutam.2015.03.073`.

Hanson, R.E., Buckley, H.P. and Lavoie, P., 2012. "Aerodynamic optimization of the flat-plate leading edge for experimental studies of laminar and transitional boundary layers". *Experiments in fluids, Springer*, Vol. 53, No. 4, pp. 863–871. doi:10.1007/s00348-012-1324-2.

Herbert, T., 1988. "Secondary Instability Of Boundary Layers". *Annual Review of Fluid Mechanics*, Vol. 20, No. 1, pp. 487–526. ISSN 00664189. doi:10.1146/annurev.fluid.20.1.487. URL `http://fluid.annualreviews.org/cgi/doi/10.1146/annurev.fluid.20.1.487`.

Juniper, M.P., Hanifi, A. and Theofilis, V., 2014. "Modal stability theory". *Applied Mechanics Reviews*, Vol. 66, No. 2. ISSN 00036900. doi:10.1115/1.4026604.

Kachanov, Y.S. and Levchenko, V.Y., 1984. "The resonant interaction of disturbances at laminar-turbulent transition in a boundary layer". *Journal of Fluid Mechanics*, Vol. 138, No. 1984, pp. 209–247. ISSN 14697645. doi:10.1017/S0022112084000100.

Klebanoff, P.S. and Tidstrom, K.D., 1972. "Mechanism by which a two-dimensional roughness element induces boundary-layer transition". *Physics of Fluids*, Vol. 15, No. 7, pp. 1173–1188. ISSN 10706631. doi:10.1063/1.1694065.

Klebanoff, P.S., Tidstrom, K.D. and Sargent, L.M., 1962. "The three-dimensional nature of boundary-layer instability". *Journal of Fluid Mechanics*, Vol. 12, No. 1, pp. 1–34. ISSN 14697645. doi:10.1017/S0022112062000014.

Methel, J., Forte, M., Vermeersch, O. and Casalis, G., 2022. "Experimental investigation on the effect of forward-facing steps and gaps combined with wall suction on boundary layer transition". *Experiments in Fluids*, Vol. 63, No. 1, pp. 1–17. ISSN 14321114. doi:10.1007/s00348-021-03361-x. URL `https://doi.org/10.1007/s00348-021-03361-x`.

Rossiter, J.E., 1964. "Wind-tunnel experiments on the flow over rectangular cavities at subsonic and transonic speeds". *Reports and Memoranda No. 3438 - Aeronautical Research Council - Ministry of Aviation*.

Saric, W.S., 1990. "Low-speed experiments: Requirements for stability measurements". In *Instability and Transition*, Springer-Verlag, New York, Vol. 1 of *ICASE/NASA LaRC*, pp. 162–174. ISBN 978-1-4612-8008-8. doi:10.1007/978-1-4612-3430-2.

Saric, W.S., Reed, H.L. and Kerschen, E.J., 2002. "Boundary-layer receptivity to freestream disturbances". *Annual Review of Fluid Mechanics*, Vol. 34, No. 1, pp. 291–319. doi:10.1146/annurev.fluid.34.082701.161921. URL `https://doi.org/10.1146/annurev.fluid.34.082701.161921`.

Sarohia, V., 1977. "Experimental investigation of oscillations in flows over shallow cavities". *AIAA Journal*, Vol. 15, No. 7, pp. 984–991. ISSN 00011452. doi:10.2514/3.60739.

Schlichting, H., 1979. *Boundary-Layer Theory*. McGraw-Hill series in mechanical engineering.

Schubauer, G.B. and Skramstad, H.K., 1948. "Laminar boundary-layer oscillations and transition on a flat plate". *National Advisory Committee for Aeronautics - Report No. 909*.

Smith, A.M.O. and Gamberoni, N., 1956. "Transition, pressure gradient, and stability theory". Technical Report ES 26388, Douglas Aircraft Division.

Tani, I., Iuchi, M. and Yamamoto, K., 1954. "Further experiments on the effect of a single roughness element on boundary-layer transition". *Report of the Institute of Science and Technology, University of Tokyo*, Vol. 8, pp. 171–178.

van Ingen, J.L., 1956. "A suggested semi-empirical method for calculation of the boundary layer transition region". *Technische Hogeschool Vliegtuigbouwkunde - Report V.T.H.-74*.

Victorino, V.B., Aguirre, F.O. and Medeiros, M.A., 2023. *Gap induced boundary layer transition*. doi:10.2514/6.2023-3997.

Wang, Y.X. and Gaster, M., 2005. "Effect of surface steps on boundary layer transition". *Experiments in Fluids*, Vol. 39, No. 4, pp. 679–686. ISSN 07234864. doi:10.1007/s00348-005-1011-7.

9. RESPONSIBILITY NOTICE

The following text, properly adapted to the number of authors, must be included in the last section of the paper:
The author(s) is (are) the only responsible for the printed material included in this paper.